



# Functionalized Magnetic Mesoporous Silica Nanoparticle-Supported Palladium Catalysts for Carbonylative Sonogashira Coupling Reactions of Aryl Iodides

Suzana Natour and Raed Abu-Reziq\*<sup>[a]</sup>

Magnetic mesoporous silica nanoparticles (MMSN) were prepared and used as a support for palladium catalysts. MMSN with a surface area of  $1909 \text{ m}^2 \text{ g}^{-1}$  were synthesized by a nano-emulsification process involving the dispersion of hydrophobic magnetite nanoparticles in chloroform in the presence of cetyltrimethylammonium bromide, followed by the addition of tetraethoxysilane and its polycondensation by a sol-gel route. The MMSN were modified with phosphine and N-heterocyclic

carbene-based ligands, which provided coordination sites for conjugation with a palladium catalyst. These modified particles were fully characterized and employed as catalyst nanosupports. The palladium catalyst was immobilized on the surface and within the pores of MMSN and applied in copper-free carbonylative Sonogashira coupling reactions of aryl iodides with terminal alkynes.

## Introduction

Of the transition metal catalysts, palladium is arguably the most widely utilized in organic transformations, including oxidation,<sup>[1]</sup> alkylation,<sup>[2]</sup> hydrogenation,<sup>[3]</sup> hydroformylation,<sup>[4]</sup> carbonylation,<sup>[5]</sup> and cross-coupling reactions.<sup>[6]</sup>

Palladium-mediated catalytic transformations are subject to avid attention from both industrial and academic communities. They play a crucial part in constructing and introducing functional groups such as esters, carbonyls, amides, amines, and alkynes and in C–C bond formation. These groups are indispensable and ubiquitous building blocks in organic chemistry, pharmaceuticals, and agrichemicals.<sup>[7]</sup>

The carbonylation reaction is a robust and direct catalytic transformation through which aromatic carbonyl compounds are attained. Of these compounds,  $\alpha,\beta$ -alkynyl ketones have gained considerable attention as they appear in myriad biologically active molecules and may serve as synthetic intermediates in natural product syntheses.<sup>[8]</sup> In this regard, several routes have been adopted for the synthesis of alkynes.<sup>[5, 9]</sup> A prevalent path involves alkynyl organometallic reagents with acid chloride.<sup>[10]</sup> However, an alternative and more atom-economic protocol for the preparation of such compounds is the palladium-catalyzed direct carbonylative Sonogashira coupling

reaction of aryl iodides with terminal alkynes in the presence of the simplest C1 unit and atom-efficient carbon monoxide.

The first palladium-catalyzed carbonylative Sonogashira reaction was reported by Kobayashi and Tanaka in 1981.<sup>[11]</sup> Customarily, this reaction requires copper co-catalyst and a high pressure of carbon monoxide. Accordingly, many enhancements and various modifications of this catalytic transformation have been established. For example, Ahmed and Mori reported a direct palladium-catalyzed carbonylative Sonogashira coupling reaction of aryl iodides with terminal alkynes under atmospheric pressure of carbon monoxide without copper co-catalyst.<sup>[12]</sup> In another study, Yang and co-workers showed a palladium-catalyzed copper-free carbonylative Sonogashira reaction of aryl iodides.<sup>[13]</sup> Fukuyama et al., reported an additional copper-free route for the synthesis of alkynes in ionic liquids.<sup>[14]</sup>

Even though palladium-catalyzed carbonylative Sonogashira coupling reactions exhibit high activities in homogeneous systems, there are difficulties in the isolation and recovery of the catalyst from the reaction mixture that may lead to contamination of the desired product. Consequently, great attention has been paid to the development of more environmentally benign systems such as heterogeneous catalysts, in which the catalytic species are supported on a solid support.<sup>[15]</sup> In this regard, supported palladium catalysts have been investigated intensively due to their chemical robustness, economic aspects, reusability, and broad utilization in many essential catalytic transformations.

To the best of our knowledge, to date only a few solid catalytic systems based on immobilized palladium catalysts have been applied in carbonylative Sonogashira coupling reactions. Such solid supports are based on cross-linked co-polymer-supported ionic liquid,<sup>[16]</sup> mesoporous silica MCM-41,<sup>[17]</sup> and bare magnetite particles.<sup>[18]</sup>

[a] S. Natour, Dr. R. Abu-Reziq  
Institute of Chemistry, Casali Center of Applied Chemistry  
Center for Nanoscience and Nanotechnology  
The Hebrew University of Jerusalem  
Jerusalem 9190401 (Israel)  
Fax: (+ 972) 2-6585469  
E-mail: Raed.Abu-Reziq@mail.huji.ac.il

Supporting Information for this article is available on the WWW under <http://dx.doi.org/10.1002/cctc.201500356>.

This publication is part of a Special Issue on Palladium Catalysis. To view the complete issue, visit: <http://onlinelibrary.wiley.com/doi/10.1002/cctc.v7.14/issuetoc>

Conventional heterogeneous catalysts are known to be less active than their homogeneous counterparts. Hence, nanocatalysis, a discipline that merges the merits of both the homogeneous and heterogeneous worlds, has been developed.<sup>[19]</sup> As a part of this field, which is directed towards developing highly efficient and recyclable catalysts, we report herein a nanocatalytic system based on the immobilization of palladium on modified magnetic mesoporous silica nanoparticles (MMSN) and its utilization in the carbonylative Sonogashira coupling reaction.

Mesoporous silica nanoparticles (MSN), containing pores with diameters in the range of 2–50 nm, have burgeoned as powerful and attractive functional materials in the field of chemistry and nanoscience.<sup>[20]</sup> MSN with controlled size and morphology display attractive properties such as high specific surface area with ample Si–OH bonds at the surface, high thermal, chemical, and mechanical stability, low toxicity, and high compatibility,<sup>[21]</sup> making them ideal candidates for a number of applications.<sup>[22]</sup> Owing to their nanometric dimensions, the isolation of MSN from reaction media is generally challenging. A commonly used strategy is the incorporation of magnetic nanoparticles such as magnetite nanoparticles (MNP) into the silica network to impart superparamagnetic properties to MSN that enable their isolation by simple application of an external magnetic field. In addition to the facile and expeditious isolation process, the magnetic nanoparticles have proven highly efficient as a catalyst support owing to their low toxicity and cost, high stability, and high surface area-to-volume ratio.<sup>[23]</sup> However, MNP will agglomerate over time and even oxidize if exposed to the atmosphere for a long period of time, leading to the loss of the distinctive magnetization. Therefore, deposition of silica on the MNP may prevent such undesirable features.

In the present work, MSN with hydrophobic MNP incorporated into the core of the silica framework (MMSN) were fabricated by a sol–gel route under basic conditions by using tetraethoxysilane (TEOS) as the silane monomer, MNP, and cetyltrimethylammonium bromide (CTAB) as both stabilizer and mesostructure-templating surfactant agent. The MMSN were then modified with various functional groups such as phosphine ligands and N-heterocyclic carbenes (NHCs) and utilized as nanosupports for the immobilization of palladium species. The synthesis, characterization, and catalytic activity of the supported palladium in the model reaction, the carbonylative Sonogashira coupling of aryl iodides and terminal alkynes, are described here. The catalyst was recovered from the reaction media and recycled efficiently by applying an external magnetic field.

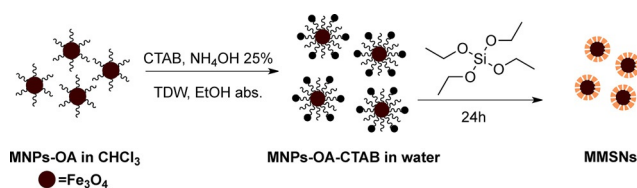
## Results and Discussion

### Synthesis of MMSN ( $\text{Fe}_3\text{O}_4@m\text{SiO}_2$ )

MMSN are inorganic materials generally prepared by deposition of a mesoporous silica layer onto MNP. In this process, various structure agents and co-agents are utilized to transfer hydrophobic MNP from the oil phase to the aqueous phase. In

addition, bases are used for the hydrolysis of the silane monomers to afford the silica matrix. For the synthesis of MMSN, our study began with the synthesis of hydrophobic oleic acid-coated MNP (MNP-OA). Various techniques have been broadly utilized for the synthesis of MNP.<sup>[24]</sup> MNP-OA were readily prepared in a one-pot reaction by co-precipitation of iron salts and ferric and ferrous chlorides at 85–90 °C in a basic aqueous medium in an inert atmosphere according to Massart's method,<sup>[25]</sup> followed by the addition of oleic acid. The pure superparamagnetic MNP were spherical in shape with an average diameter of 15–20 nm, as substantiated by transmission electron microscopy (TEM, Figure S1). Such particles have a high tendency to agglomerate to diminish the high energy derived from the high surface area-to-volume ratio. Moreover, non-modified MNP are poorly dispersible in any medium. Thus, to avoid this restriction, numerous surface-coating agents and capping methods were utilized. In this case, the MNP were stabilized with oleate groups, which coordinated with iron ions present on the surface of the MNP through the oxygen atoms of the carboxylate. The oleate groups, in addition to sterically stabilizing the MNP, enhanced the solubility of MNP in solvents such as chloroform.

The dispersion of MNP-OA in chloroform was utilized in the preparation of the MMSN. The synthetic approach for establishing the MMSN is depicted in Scheme 1.



Scheme 1. Synthesis of MMSN  $\text{Fe}_3\text{O}_4@m\text{SiO}_2$ . TDW = triple distilled water.

Practically, the entrapment of the MNP-OA within the silica network was achieved by emulsification of the MNP in aqueous solution with use of a templating surfactant CTAB that transferred the MNP-OA from the oil phase to the aqueous phase by micellar dispersion. Subsequently, the mesoporous silica network was attained by the slow addition of the silica precursor TEOS, which was hydrolyzed and condensed in basic medium by the conventional sol–gel process.

The surface morphology of MMSN was probed by scanning electron microscopy (SEM) and TEM analyses, which verified the formation of spherical porous silica nanoparticles with MNP in the core of the network (Figure 1 a and b, respectively).

The particle size distribution and zeta potential of the unfunctionalized MMSN were analyzed by using dynamic light scattering (DLS) and Nano-ZetaSizer instruments, respectively, as depicted in Figure 2. These analyses revealed the formation of poly-dispersed MMSN with an average particle size of 304 nm and zeta potential of –27.8 mV. The negative zeta potential charge was due to deprotonation of the silanol groups present on the surface. Furthermore, the absolute value of the

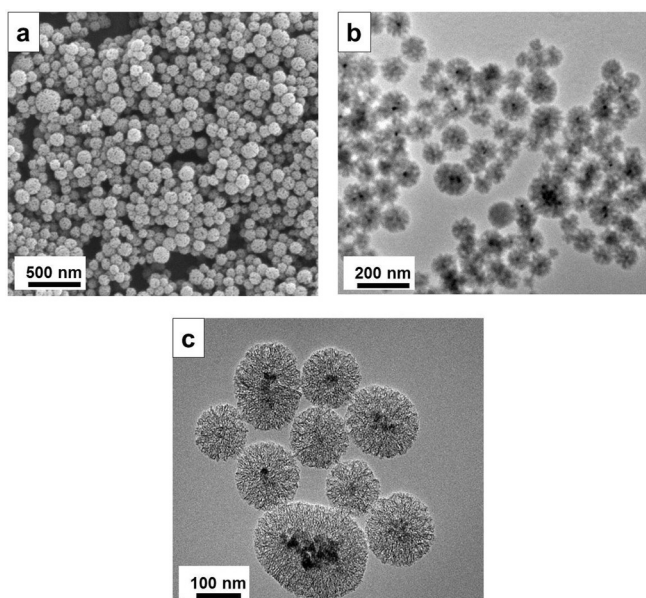


Figure 1. a) SEM and b, c) TEM micrographs of MMSN.

zeta potential indicated that the MMSN were stable owing to the moderate to high degree of the electrostatic repulsion between adjacent MMSN.

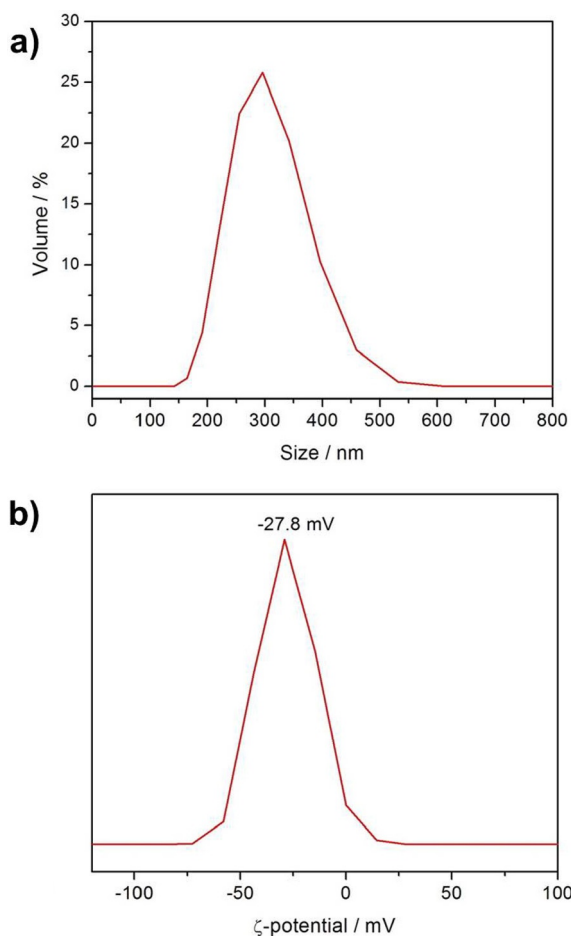


Figure 2. a) Particle size distribution and b) zeta ( $\zeta$ ) potential graph of MMSN.

To obtain the mesostructure and gain access to the pores, the templating surfactant had to be removed. This could be achieved by calcination, however, this method is associated with pore size reduction, a low degree of condensation of the silica network, and particle agglomeration. In this work, we have produced MMSN with a higher surface area than reported previously,  $1000 \text{ m}^2 \text{ g}^{-1}$ , without adopting the calcination process. The specific surface area of the MMSN evaluated by Brunauer–Emmett–Teller (BET) analysis was approximately  $1909 \text{ m}^2 \text{ g}^{-1}$  and the pore volume and diameter according to Barrett–Joyner–Halenda (BJH) calculations were  $0.216 \text{ cm}^3 \text{ g}^{-1}$  and  $1.89 \text{ nm}$ , respectively. The nitrogen adsorption–desorption isotherm of the MMSN is shown in Figure S2.

The chemistry of the silica matrix was investigated further by using solid-state  $^{29}\text{Si}$  cross polarization magic angle spinning ( $^{29}\text{Si}$  CP-MAS) NMR spectroscopy (Figure 3). Pure MSN, synthesized in the same manner as MMSN, exhibited two distinct signals at  $\delta = -100.07$  and  $-110.51$  ppm. These signals were attributed to isolated silanol ( $\text{Q}^3$ ) and siloxane groups ( $\text{Q}^4$ ), respectively.

The composition of the MMSN was probed further by X-ray powder diffraction (XRD). The XRD pattern of the MMSN (Figure 4b) displayed the characteristic peaks of the MNP at  $2\theta = 18.1, 30.1, 35.5, 43.4, 53.8, 57.4,$  and  $62.8^\circ$ , which were identical to the observed peaks of the pure MNP (Figure 4a). The broad

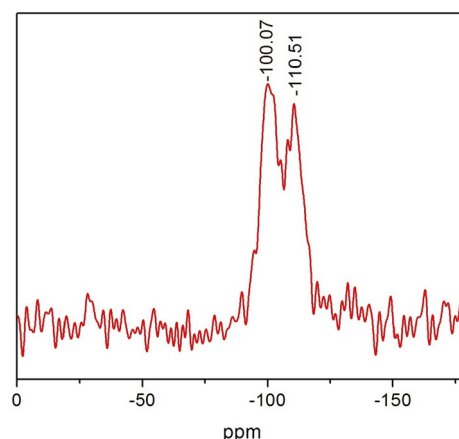


Figure 3.  $^{29}\text{Si}$  CP-MAS NMR spectrum of MSN.

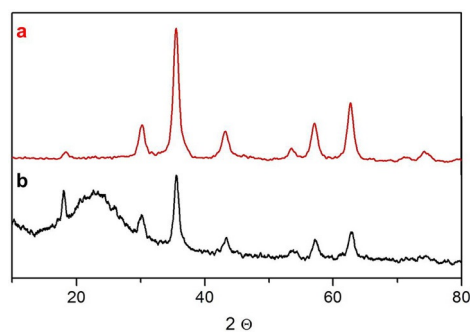
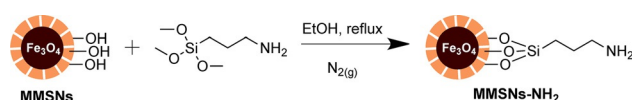


Figure 4. XRD pattern of a) pure magnetite and b) MMSN.

peak in the range  $2\theta = 18\text{--}28^\circ$  was assigned to the amorphous silica network.

### Preparation and characterization of amine-functionalized MMSN (MMSN-NH<sub>2</sub>)

Surface modification of MMSN can be achieved mostly through a post-synthetic approach, such as grafting or co-condensation. The amine functionality was introduced by reacting (3-aminopropyl)trimethoxysilane (3-APTMS) with MMSN in ethanol at 80 °C in an inert atmosphere. The functionalization occurred through condensation of the methoxy groups with the surface silanol groups, resulting in the loss of methanol (Scheme 2). The functionalization step did not affect the morphology or particle size distribution according to SEM, TEM, and DLS analyses (Figures S3 a, b, and S4 respectively).



Scheme 2. Amine-functionalized MMSN.

Further analysis to verify the presence of the organic units on the MMSN was conducted by using thermogravimetric analysis (TGA) in the temperature range of 25–950 °C in an inert atmosphere. TGA results from pure MNP, MNP-OA, MMSN, and MMSN-NH<sub>2</sub> are shown in Figure 5. Oleic acid-stabilized MNP exhibited an increase in the organic content with 19% weight loss (Figure 5 b), in comparison to the pure MNP, which underwent 3.5% weight loss (Figure 5 a); this was attributed to solvent residues and absorbed moisture. For MMSN the weight loss of 29.73% (Figure 5 c) could be ascribed to the removal of surfactant molecules (CTAB), which decomposed in the temperature range 243–273 °C. Notably, CTAB was also encapsulated within the pores, generating interactions with the domestic surface of the mesoporous silica framework. Hence, higher temperatures were required for the decomposition of the

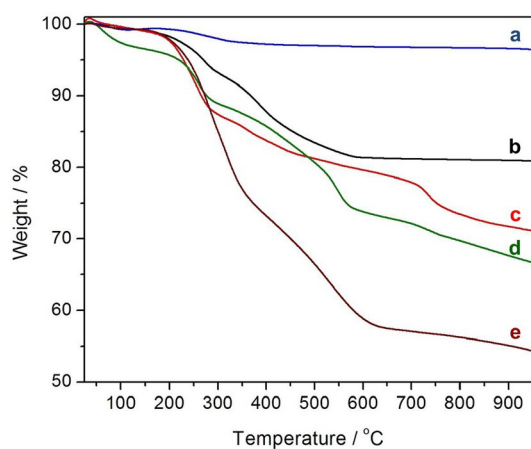


Figure 5. TGA curves of a) pure MNP, b) MNP-OA, c) MMSN, d) MMSN-NH<sub>2</sub>, and e) MMSN-N-(PPh<sub>2</sub>)<sub>2</sub>.

CTAB molecules concealed within the pores. Additionally, the weight loss at temperatures above 500 °C was due to thermal dehydroxylation and condensation of the silanol groups on the internal surface of the MSN to form siloxane groups. To exclusively remove the templating surfactants and residues of the unreacted silica precursors, thermal treatment such as calcination would be required. However, this process could change the morphology, collapse the pore network, and may lead to dehydroxylation of the surface silanol groups resulting in particle agglomeration.

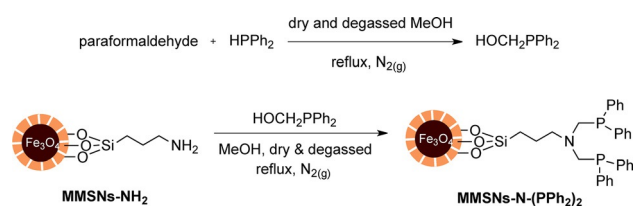
After functionalizing the MMSN with 3-APTMS, 33.65% weight loss was observed (Figure 5 d), which indicated that more organic content, in this case  $\equiv\text{Si}-(\text{CH}_2)_3\text{NH}_2$ , was present.

The IR spectra of MMSN and MMSN-NH<sub>2</sub> are shown in Figure S5. The MMSN exhibited absorption peaks at 1110 cm<sup>-1</sup> and at intervals of 3100–3707 cm<sup>-1</sup>, which were attributed to the asymmetrical stretching of Si–O–Si and Si–OH vibrations, respectively (Figure S5 a). In addition, absorption bands at 1643 and 2851–2920 cm<sup>-1</sup> were assigned to the C=C and C–H stretching vibrations, respectively, of the oleate groups stabilizing the MNP. The amine-functionalized MMSN exhibited similar absorption peaks to MMSN, in addition to peaks at 1550 and 1090 cm<sup>-1</sup>, which were ascribed to the N–H bending and C–N stretching vibrations, respectively (Figure S5 b).

### Preparation and characterization of phosphonated MMSN-NH<sub>2</sub> (MMSN-N-(PPh<sub>2</sub>)<sub>2</sub>)

Palladium complexes with phosphines as ligands have been utilized in various carbonylation reactions, providing high catalytic efficiency and selectivity. In our study, we supported a phosphine ligand on MMSN by reacting MMSN-NH<sub>2</sub> with (diphenylphosphino)methanol, prepared from diphenylphosphine and paraformaldehyde, in dry and degassed methanol. The synthetic process of MMSN-N-(PPh<sub>2</sub>)<sub>2</sub> is depicted in Scheme 3.

After phosphonation of MMSN-NH<sub>2</sub>, its morphology, shape, and particle size distribution were retained in MMSN-N-(PPh<sub>2</sub>)<sub>2</sub>, as observed in SEM, TEM (Figure S6 a and b, respectively), and DLS analyses (Figure S7). Moreover, TGA of MMSN-N-(PPh<sub>2</sub>)<sub>2</sub> displayed a higher organic content with a weight loss of 45.8% (Figure 5 e) compared to the non-phosphonated system MMSN-NH<sub>2</sub>, which ascertained that the phosphonation reaction indeed occurred. IR spectroscopy revealed similar absorption bands as in previous systems, in addition to absorption peaks at 1650, 1480, and 1080 cm<sup>-1</sup>, which were assigned to the stretching vibrations of the aromatic C=C and C–N bonds (Figure S5 c).

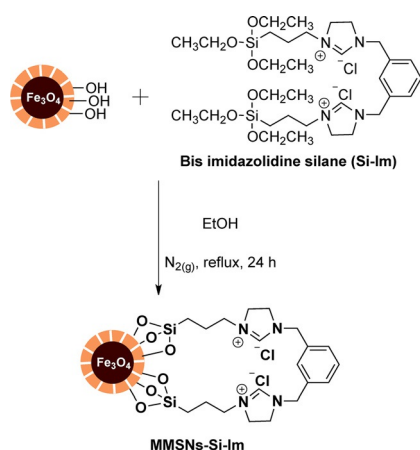


Scheme 3. Preparation of MMSN-N-(PPh<sub>2</sub>)<sub>2</sub>.

### Preparation and characterization of bis-imidazolidine-based NHC supported on MMSN (MMSN-Si-NHC)

NHCs have been established as efficient ligands in transition metal-catalyzed reactions due to their excellent electron-donating ability as strong  $\sigma$  donors. NHC-metal complexes are ubiquitous in organometallic chemistry and have been utilized in a broad range of reactions such as carbonylation and other C–C and C–N coupling, polymerization, and hydrogenation reactions.<sup>[26]</sup>

We have prepared an additional catalyst support based on the immobilization of 1,1'-[1,3-phenylenebis(methylene)]bis[3-[3-(triethoxysilyl)propyl]-4,5-dihydro-1*H*-imidazol-3-ium] chloride [bis-imidazolidine silane (Si-Im)] on the surface of MMSN. The preparation of this system was initiated by the synthesis of Si-Im with  $\alpha,\alpha$ -dichloro-*m*-xylene and triethoxy-3-(2-imidazolin-1-yl)propylsilane in ethanol at 80 °C. Subsequently, the Si-Im was grafted on the surface of MMSN through reaction of the triethoxysilane groups of the Si-Im ligand with the surface hydroxyl groups of the MMSN in ethanol for 24 h at 80 °C (Scheme 4). The resulting system MMSN-Si-Im showed no significant change in particle size, as verified in TEM and DLS analyses (Figure S8 a and b, respectively).



Scheme 4. Preparation of MMSN-Si-Im.

Zeta potential measurements of the MMSN-Si-Im revealed a potential of +25.8 mV, confirming the immobilization and the presence of positively charged imidazolidine groups on the surface of the MMSN (Figure 6a). Additionally, TGA verified the presence of organic groups of the Si-Im on the MMSN, by revealing a weight loss of 38.3% (Figure 6b).

IR analysis of the MMSN-Si-Im (Figure 7b) showed the characteristic absorption bands of Si-Im functional groups (Figure 7a), C–N at 1078  $\text{cm}^{-1}$  and C=C at 1445 and 1654  $\text{cm}^{-1}$ . In addition, the typical asymmetric stretching vibrations of the Si–O–Si and Si–OH bonds could be distinctly identified.

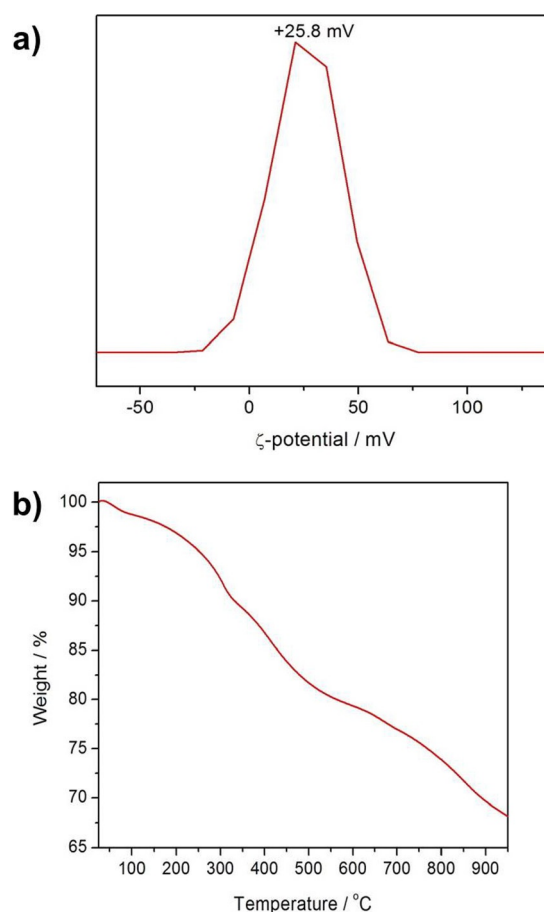


Figure 6. a) Zeta potential graph and b) TGA curve of MMSN-Si-Im.

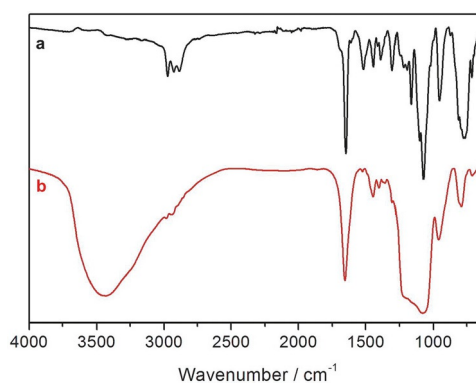
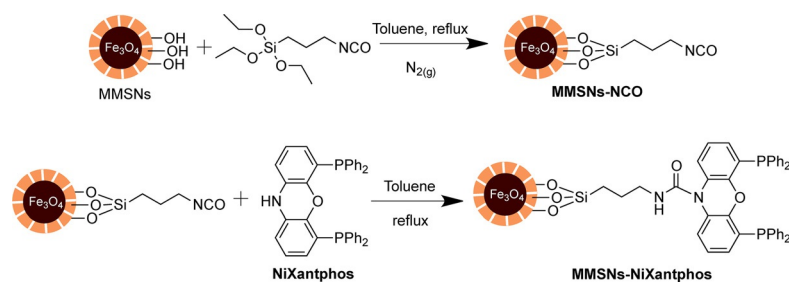


Figure 7. IR spectra of a) Si-Im and b) MMSN-Si-Im.

### Preparation and characterization of NiXantphos-supported MMSN (MMSN-NiXantphos)

The MMSN-supported NiXantphos ligand 4,6-bis(diphenylphosphino)phenoxazine was prepared in a similar manner to the previous systems. MMSN was initially modified with isocyanate groups by a condensation reaction of –OH groups on the surface of MMSN with (3-isocyanatopropyl)triethoxysilane. Then, the phenoxazine-based ligand NiXantphos was reacted with the isocyanate moiety on the MMSN. The synthetic route is described in Scheme 5.

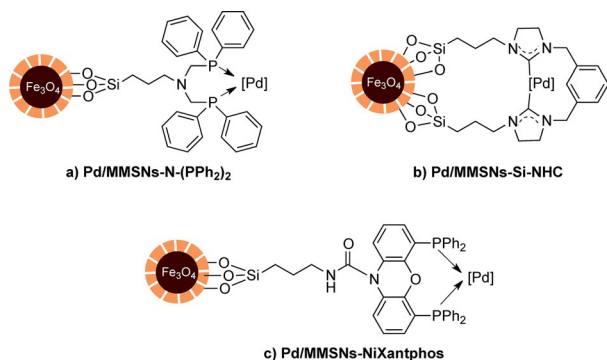


Scheme 5. Preparation of MMSN-NiXantphos.

TGA analysis of (3-isocyanatopropyl)triethoxysilane-modified MMSN (Figure S9a) revealed a 41% weight loss, whereas MMSN-NiXantphos displayed a higher weight loss of 50% (Figure S9b), indicating attachment of the NiXantphos ligand. The morphology and size distribution of MMSN-NiXantphos remained intact, as shown in TEM and DLS analyses (Figure S10a and b).

### Immobilization of palladium catalyst

To evaluate the efficiency of the modified MMSN in catalysis, palladium-based catalysts were supported on the functionalized MMSN. Several supported palladium systems based on palladium(II) and palladium(0) on MMSN-*N*-PPh<sub>2</sub>, MMSN-Si-NHC, and MMSN-NiXantphos were accomplished. Palladium(II) and palladium(0) grafted on the modified MMSN, through coordination with the phosphine or carbene groups, were synthesized by reacting palladium catalysts with functionalized MMSN in toluene at room temperature for 24 h (Scheme 6). Pd/MMSN-Si-NHC was prepared by initially reacting MMSNs-Si-Im with an excess of a strong base, potassium *tert*-butoxide, in dry methanol and an inert atmosphere followed by the addition of palladium precursor catalyst. Several palladium precursors such as Pd(OAc)<sub>2</sub>, Pd(cod)Cl<sub>2</sub> (cod = cyclooctadiene), and Pd(CH<sub>3</sub>CN)<sub>2</sub>Cl<sub>2</sub> were immobilized onto MMSN-*N*-(PPh<sub>2</sub>)<sub>2</sub>, MMSN-Si-NHC, and MMSN-NiXantphos. To ascertain the presence of the palladium species on the functionalized MMSN, TEM, scanning transmission electron microscopy/energy dispersive X-ray



Scheme 6. Palladium supported on a) MMSN-*N*-(PPh<sub>2</sub>)<sub>2</sub>, b) MMSN-Si-NHC, and c) MMSN-NiXantphos.

spectroscopy (STEM-EDS), XRD and X-ray photoelectron spectroscopy (XPS) analyses were conducted.

TEM (Figure 8) and STEMEDS (Figure 9) of the aforementioned systems clearly showed the existence of palladium species and the entrapped iron components of MNP-OA within the core of the silica network.

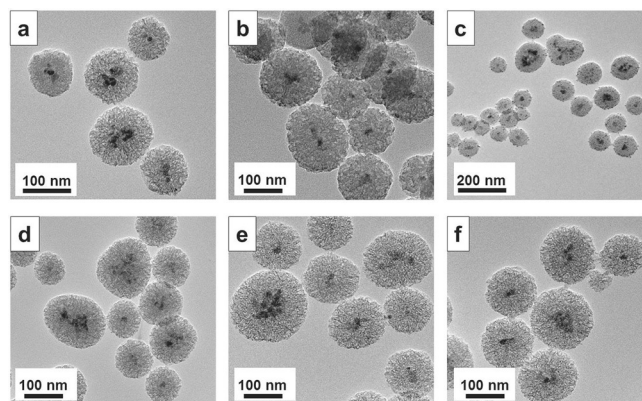


Figure 8. TEM micrographs of a) Pd(OAc)<sub>2</sub>/MMSN-*N*-(PPh<sub>2</sub>)<sub>2</sub>, b) Pd(cod)Cl<sub>2</sub>/MMSN-*N*-(PPh<sub>2</sub>)<sub>2</sub>, c) Pd<sup>0</sup>/MMSN-Si-NHC, d) Pd(cod)Cl<sub>2</sub>/MMSN-Si-NHC, e) Pd(OAc)<sub>2</sub>/MMSN-NiXantphos, and f) Pd(CH<sub>3</sub>CN)<sub>2</sub>Cl<sub>2</sub>/MMSN-NiXantphos.

XPS analysis (Figure S11) was utilized to identify the oxidation state of the palladium on the modified MMSN. Pd(OAc)<sub>2</sub>/MMSN-*N*-(PPh<sub>2</sub>)<sub>2</sub> had characteristic peaks corresponding to palladium(II) species (Figure S11 a). The peaks centered at 337.0 and 342.1 eV were attributed to Pd3d<sub>5/2</sub> and Pd3d<sub>3/2</sub>, respectively. Pd<sup>0</sup>/MMSN-Si-NHC displayed peaks at 335.1 and 340.5 eV, which were attributed to palladium(0) (Figure S11 b).

Presence of palladium(0) on MMSN-Si-NHC was also proved by XRD analysis. Four peaks at 2θ = 39.71, 46.00, 66.36, and 74.08° were assigned to the face-centered cubic palladium crystal structure and the (100), (200), (220), and (311) reflections, respectively (Figure S12).

### Catalysis

To comprehend and evaluate the catalytic efficacy of the systems, we began by testing the as-prepared catalysts Pd/MMSN-*N*-(PPh<sub>2</sub>)<sub>2</sub> in the model carbonylative Sonogashira reaction of 4-iodoanisole and phenylacetylene with triethylamine as base.

Different reaction temperatures, times, and carbon monoxide pressures with 1 mol% of palladium catalyst were investigated as displayed in Table 1. Among the conditions tested, a reaction temperature of 80 °C with 40 psi (1 psi = 6.89 kPa) of carbon monoxide, and reaction time of 24 h (entry 5) proved the most efficient. If the reaction was conducted with 40 or 400 psi of carbon monoxide at room temperature, no reaction

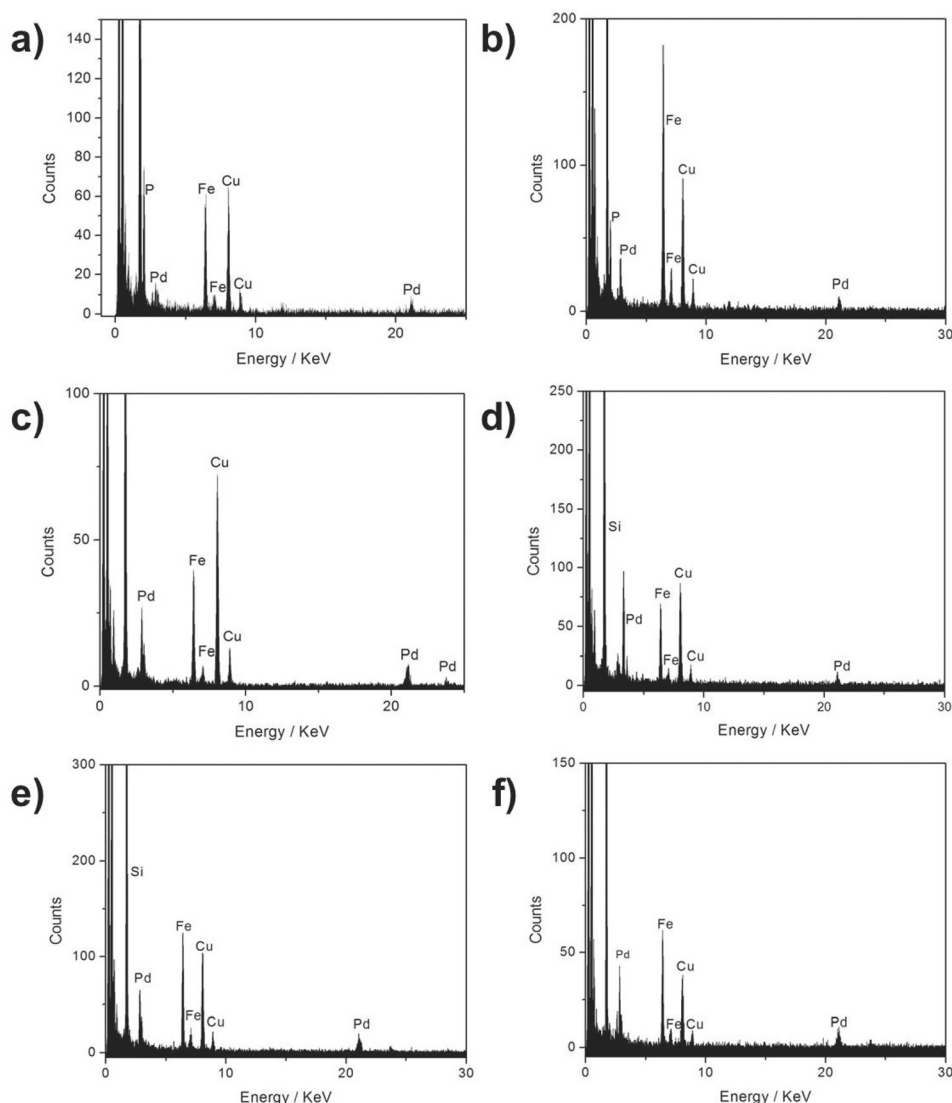
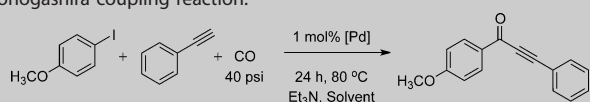


**Table 2.** Effect of solvent and palladium catalyst on the carbonylative Sonogashira coupling reaction.



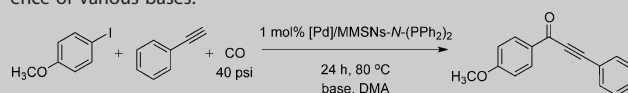
Entry	Supported ligand	Palladium precursor	Solvent	Yield <sup>[f]</sup> [%]
1	MMSN-N-(PPh <sub>2</sub> ) <sub>2</sub> <sup>[a]</sup>	Pd(OAc) <sub>2</sub>	DMA	94
2			toluene	35
3			DMSO	86
4			DMF	84
5			acetonitrile	45
6			H <sub>2</sub> O	57
7			[BmIm]PF <sub>6</sub>	75
8	MMSN-N-(PPh <sub>2</sub> ) <sub>2</sub> <sup>[b]</sup>	Pd(cod)Cl <sub>2</sub>	toluene	72
9			DMSO	56
10			DMF	43
11			acetonitrile	29
12			[BmIm]PF <sub>6</sub>	81
13			DMA	96
14	MMSN-Si-NHC <sup>[c]</sup>	Pd(cod)Cl <sub>2</sub>	toluene	48
15			DMSO	86
16			DMF	78
17			acetonitrile	51
18			DMA	82
19			[BmIm]PF <sub>6</sub>	61
20	MMSN-Si-NHC <sup>[d]</sup>	Pd(OAc) <sub>2</sub>	toluene	82
21			DMSO	90
22			acetonitrile	28
23			DMA	88
24	MMSN-NiXantphos <sup>[e]</sup>	Pd(OAc) <sub>2</sub>	toluene	63
25			DMSO	86
26			acetonitrile	88
27			DMA	94
28	MMSN-NiXantphos <sup>[e]</sup>	Pd(CH <sub>3</sub> CN) <sub>2</sub> Cl <sub>2</sub>	toluene	64
29			DMSO	73
30			acetonitrile	86
31			DMA	88

[a] 1 g Pd<sup>II</sup>/MMSN-N-(PPh<sub>2</sub>)<sub>2</sub> suspension containing  $5.9 \times 10^{-3}$  mmol [Pd], 0.59 mmol 4-iodoanisole, 0.708 mmol phenylacetylene, 0.59 mmol Et<sub>3</sub>N, and 4 mL solvent. [b] 1 g Pd<sup>II</sup>/MMSN-N-(PPh<sub>2</sub>)<sub>2</sub> suspension containing  $5.25 \times 10^{-3}$  mmol [Pd], 0.525 mmol 4-iodoanisole, 0.63 mmol phenylacetylene, 0.525 mmol Et<sub>3</sub>N, and 4 mL solvent. [c] 1 g Pd<sup>II</sup>/MMSN-Si-NHC suspension containing  $4.67 \times 10^{-3}$  mmol [Pd], 0.46 mmol 4-iodoanisole, 0.56 mmol phenylacetylene, 0.46 mmol Et<sub>3</sub>N, and 4 mL solvent. [d] 1 g Pd<sup>II</sup>/MMSN-Si-NHC suspension containing  $5.9 \times 10^{-3}$  mmol [Pd], 0.59 mmol 4-iodoanisole, 0.708 mmol phenylacetylene, 0.59 mmol Et<sub>3</sub>N, and 4 mL solvent. [e] 1 g Pd<sup>II</sup>/MMSN-NiXantphos suspension containing  $5.14 \times 10^{-3}$  mmol [Pd], 0.514 mmol 4-iodoanisole, 0.62 mmol phenylacetylene, 0.514 mmol Et<sub>3</sub>N, and 4 mL solvent. [f] Determined by <sup>1</sup>H NMR spectroscopy and GC analyses.

reaction conditions of 40 psi carbon monoxide, triethylamine as base, 80 °C, and a reaction time of 24 h. The results are summarized in Table 4.

With iodobenzene as the substrate, 85% yield was obtained. 80 and 81% yield were acquired when the aryl iodide was substituted with moderately and weakly electron-withdrawing groups, respectively (Table 4, entries 2 and 6), whereas a strongly electron-withdrawing group afforded 50% yield (entry 5). On the other hand, electron-donating groups afforded moderate yields (entries 3 and 4). We then investigated a few terminal alkynes containing different groups in the carbonylative reaction with 4-iodoanisole. With 1-ethynyl-4-fluorobenzene, 78% yield

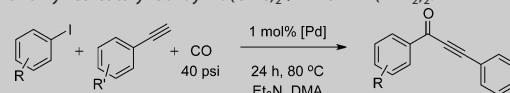
**Table 3.** Carbonylative Sonogashira reaction of 4-iodoanisole and phenylacetylene catalyzed by MMSN-N-(PPh<sub>2</sub>)<sub>2</sub>-supported palladium in the presence of various bases.



Entry	Palladium precursor	Base	Yield <sup>[c]</sup> [%]
1	Pd(OAc) <sub>2</sub> <sup>[a]</sup>	Et <sub>3</sub> N	94
2		K <sub>2</sub> CO <sub>3</sub>	84
3		Cs <sub>2</sub> CO <sub>3</sub>	83
4		pyridine	13
5		NaOAc	69
6	Pd(cod)Cl <sub>2</sub> <sup>[b]</sup>	Et <sub>3</sub> N	96
7		K <sub>2</sub> CO <sub>3</sub>	34
8		Cs <sub>2</sub> CO <sub>3</sub>	83
9		pyridine	10
10		NaOAc	70

[a] 1 g Pd(OAc)<sub>2</sub>/MMSN-N-(PPh<sub>2</sub>)<sub>2</sub> suspension containing  $5.9 \times 10^{-3}$  mmol [Pd], 0.59 mmol 4-iodoanisole, 0.708 mmol phenylacetylene, 0.59 mmol base, and 4 mL DMA. [b] 1 g Pd(cod)Cl<sub>2</sub>/MMSN-N-(PPh<sub>2</sub>)<sub>2</sub> suspension containing  $5.25 \times 10^{-3}$  mmol [Pd], 0.525 mmol 4-iodoanisole, 0.63 mmol phenylacetylene, 0.525 mmol base, and 4 mL DMA. [c] Determined by <sup>1</sup>H NMR spectroscopy and GC analyses.

**Table 4.** Carbonylative Sonogashira reaction of various aryl iodides and terminal alkynes catalyzed by Pd(OAc)<sub>2</sub>/MMSN-N-(PPh<sub>2</sub>)<sub>2</sub>.



Entry	Aryl iodide	Terminal alkyne	Yield <sup>[b]</sup> [%]
1	iodobenzene	phenylacetylene	85
2	4-iodoacetophenone	phenylacetylene	80
3	3-iodotoluene	phenylacetylene	73
4	4-iodotoluene	phenylacetylene	65
5	1-iodo-4-nitrobenzene	phenylacetylene	50
6	1-chloro-4-iodobenzene	phenylacetylene	81
7	4-iodoanisole	1-ethynyl-4-fluorobenzene	78
8	4-iodoanisole	4-ethynylanisole	80
9	4-iodoanisole	4-ethynyltoluene	92

[a] 1 g Pd(OAc)<sub>2</sub>/MMSN-N-(PPh<sub>2</sub>)<sub>2</sub> suspension containing  $5.9 \times 10^{-3}$  mmol [Pd], 0.59 mmol aryl iodide, 0.708 mmol acetylene, 0.59 mmol Et<sub>3</sub>N, and 4 mL DMA. [b] Determined by <sup>1</sup>H NMR spectroscopy and GC analyses.

was attained (entry 7) whereas higher yields of 80 and 92% were reached if 4-ethynylanisole and 4-ethynyltoluene were used (entries 8 and 9).

Ensuring recyclability of the heterogeneous catalysts while maintaining the catalytic efficiency is a prominent concern in the field of catalysis. By entrapment of magnetic nanoparticles in the core of a mesoporous silica network, isolation and recovery of the catalyst is achieved easily by exposure to an external magnetic field. Thus, the recyclability of Pd(OAc)<sub>2</sub>/MMSN-N-(PPh<sub>2</sub>)<sub>2</sub> was explored and evaluated in the carbonylative Sonogashira coupling reaction of 4-iodoanisole and phenylacetylene under the optimized reaction conditions. The recyclability of the of Pd(OAc)<sub>2</sub>/MMSN-N-(PPh<sub>2</sub>)<sub>2</sub> was verified in four consecutive cycles, with some decrease in the reactivity

observed in the third and fourth cycles (Figure 10). After each catalytic reaction, the catalyst was separated readily by applying an external magnetic field (Figure 11), washed with DMA, and utilized directly in the next cycle.

After performing the catalytic reaction, leaching of the palladium species from the catalytic system was examined by inductively coupled plasma mass spectrometry measurements (ICP-MS). There was no detectable leaching of palladium. Furthermore, to prove that the catalytic system was stable and unaffected by the reaction conditions, the recovered catalyst was examined by SEM and TEM analyses. The SEM and TEM micrographs of the catalyst in Figure 12 affirmed that the morphology and size distribution after three cycles remained largely intact.

TEM (Figure 12b), EDS, and XPS analyses (Figure 13a and b) unambiguously confirmed the presence of palladium nanoparticles on the surface of the MMSN system after the carbonylation reaction, indicating that palladium(II) was reduced to palladium(0) during the catalytic reaction.

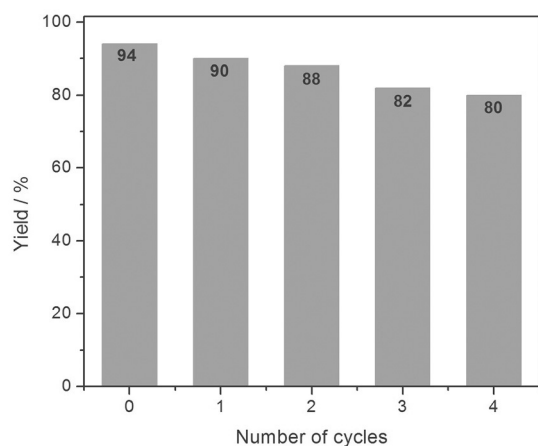


**Figure 10.** Recyclability of Pd(OAc)<sub>2</sub>/MMSN-N-(PPh<sub>2</sub>)<sub>2</sub> in the carbonylative Sonogashira coupling reaction of 4-iodoanisole and phenylacetylene.

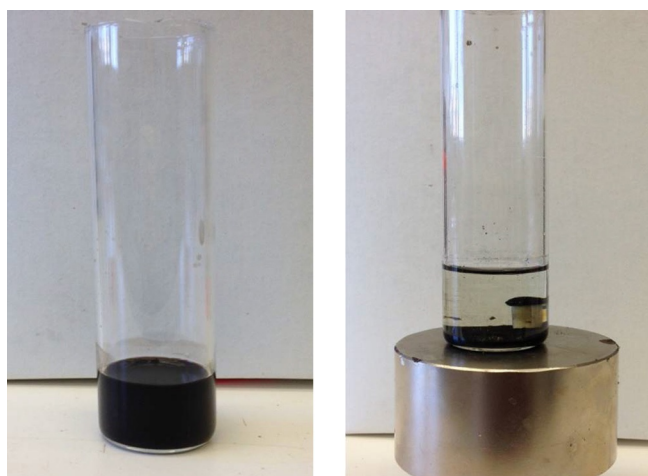


**Figure 11.** Magnetic separation of Pd(OAc)<sub>2</sub>/MMSN-N-(PPh<sub>2</sub>)<sub>2</sub> from the reaction mixture.

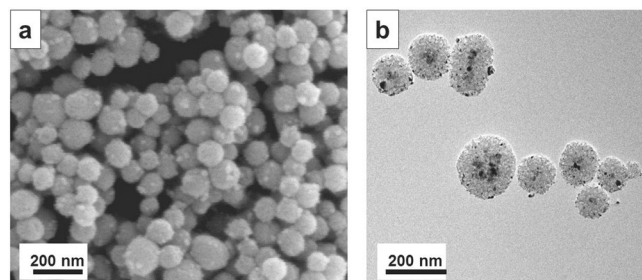


**Figure 12.** Recycled Pd(OAc)<sub>2</sub>/MMSN-N-(PPh<sub>2</sub>)<sub>2</sub> after three cycles: a) SEM and b) TEM micrographs.

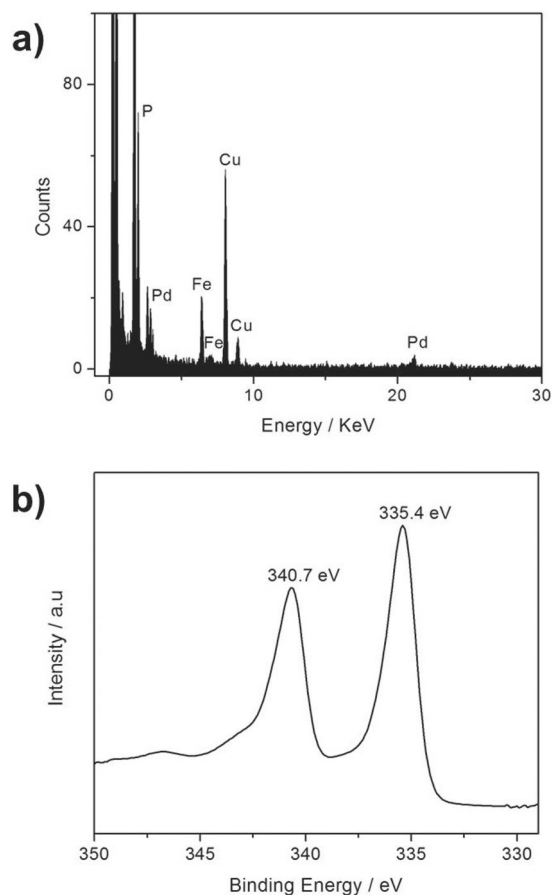


**Figure 13.** a) EDS and b) XPS analysis Pd<sup>0</sup>/MMSN-N-(PPh<sub>2</sub>)<sub>2</sub> after the carbonylative Sonogashira reaction.

## Conclusions

Highly mesoporous magnetic silica nanoparticles (MMSN) with a surface area of 1909 m<sup>2</sup>g<sup>-1</sup> were prepared without the adoption of any calcination process and utilized as catalyst nano-supports. Of the various functionalized MMSN that were prepared, palladium(II) acetate supported on MMSN-N-(PPh<sub>2</sub>)<sub>2</sub> showed high activity in the carbonylative Sonogashira coupling reaction under the optimized reaction conditions of 40 psi carbon monoxide in the presence of triethylamine as the base and dimethylacetamide as reaction solvent. Owing to the presence of magnetic nanoparticles in the core of the mes-

oporous silica nanoparticles, the catalytic system was readily isolated from the reaction mixture by simple application of an external magnetic field. The catalyst was recycled up to four times, exhibiting some decrease in the catalytic efficiency after the fourth cycle.

## Experimental Section

### Materials and methods

CTAB,  $\text{FeCl}_3 \cdot 6\text{H}_2\text{O}$ ,  $\text{FeCl}_2 \cdot 4\text{H}_2\text{O}$ ,  $\text{NH}_4\text{OH}$  25%, oleic acid, and  $\text{Pd}(\text{OAc})_2$  were purchased from Acros Fischer Scientific. TEOS was contributed by Sol-Gel Technologies and 3-APTMS (95%),  $\alpha, \alpha$ -dichloro-*m*-xylene and triethoxy-3-(2-imidazolin-1-yl)propylsilane purchased from Sigma Aldrich. All substrates for the carbonylative Sonogashira reactions were purchased from either Sigma Aldrich or Acros and used without further purification. SEM was used to determine the morphology of the MMSN system. The experiments were performed on a high-resolution scanning electron microscope (Sirion, FEI Company) with a Shottky-type field emission source and secondary electron detector. The images were scanned at a voltage of 5 kV. TEM and EDS were performed on a Tecnai (S)TEM F20 G2 instrument (FEI Company) operated at 200 kV. The IR spectra were recorded at RT in transmission mode on a PerkinElmer 65 FTIR spectrometer. TGA was performed on a Mettler Toledo TG 50 analyzer. Measurements were performed in a temperature range of 25–950 °C at a heating rate of 10 °C min<sup>-1</sup> in  $\text{N}_2$ . DLS and zeta potential were measured by using a Nano-Series Nano-ZetaSizer ZEN3600 instrument (Malvern Instruments). GC (7890 A, Agilent Technologies) with a capillary column (HP-5, 30 m) was used to determine the yields of the carbonylative Sonogashira reactions. <sup>1</sup>H NMR and <sup>13</sup>C NMR spectra were recorded on a Bruker DRX-400 instrument in  $\text{CDCl}_3$ . XRD measurements were performed on the D8 Advance diffractometer (Bruker AXS, Karlsruhe, Germany) with a goniometer radius of 217.5 mm, secondary graphite monochromator, 2° Soller slits and 0.2 mm receiving slit. Low-background quartz sample holders were filled with the powder samples. XRD patterns within the range  $2\theta = 1$  to 90° were recorded at RT by using  $\text{CuK}\alpha$  radiation ( $\lambda = 1.5418 \text{ \AA}$ ) under the following measurement conditions: tube voltage 40 kV, tube current 40 mA, step-scan mode with a step size of  $2\theta = 0.02^\circ$ , and counting time 1 s step<sup>-1</sup>. XPS measurements were performed by using a Kratos Axis Ultra X-ray photoelectron spectrometer (Kratos Analytical) with an  $\text{AlK}\alpha$  monochromatic radiation source (1486.7 eV), pass energy of 20 eV, and step size of 0.1 eV. The binding energies were calibrated to a C 1s energy of 285.0 eV. The specific surface areas were calculated by means of the BET equation by utilizing a high-speed gas sorption analyzer, Quantachrome Nova 1200e instrument.

### Preparation of MNP-OA

$\text{FeCl}_3 \cdot 6\text{H}_2\text{O}$  (11.7 g) and  $\text{FeCl}_2 \cdot 4\text{H}_2\text{O}$  (4.4 g) were dissolved and stirred mechanically in deionized  $\text{H}_2\text{O}$  (400 mL) in an inert atmosphere. The mixture was heated at 85–90 °C followed by rapid addition of  $\text{NH}_4\text{OH}$  (aq) solution (25%, 18 mL), producing a black suspension of MNP. The mixture was heated for a further 20 min, then oleic acid (18 mL) added slowly to the suspension, which was allowed to stir for a further 60 min at 85–90 °C until a black precipitate formed. The mixture was cooled to RT and the hydrophobic MNP-OA isolated by applying an external magnetic field and washing with deionized  $\text{H}_2\text{O}$  and 4 times with acetone. Finally, the MNP-OA were suspended in  $\text{CHCl}_3$  (100 mL) and sonicated for 90 min.

### Preparation of MMSN

MMSN were prepared by the addition of MNP-OA (50 mg mL<sup>-1</sup>, 1 mL) to a solution containing CTAB (0.48 g), absolute EtOH (33 mL), triple-distilled  $\text{H}_2\text{O}$  (88 mL), and concentrated  $\text{NH}_3$ (aq) solution (25 wt%, 0.1 mL). The resulting mixture was stirred mechanically for 60 min at RT, followed by the addition of TEOS (1.27 g). The reaction mixture was stirred for a further 24 h to generate the MMSN, which were isolated magnetically and washed several times with distilled  $\text{H}_2\text{O}$  and then with EtOH. The system was redispersed in EtOH (100 mL) and sonicated for 60 min.

### Preparation of MMSN-NH<sub>2</sub>

To a suspension of MMSN dispersed in EtOH (150 mL), 3-APTMS (5 mmol, 0.9 g) was added and stirred mechanically under reflux in an inert atmosphere for 24 h. The amine-modified MMSN were isolated magnetically, washed with EtOH and MeOH, and redispersed in dry, degassed MeOH (100 mL).

### Preparation of MMSN-N-(PPh<sub>2</sub>)<sub>2</sub>

Diphenylphosphine (8.05 mmol, 1.4 mL), prepared according to the literature,<sup>[27]</sup> was refluxed with paraformaldehyde (8.1 mmol, 0.24 g) in dry and degassed MeOH for 60 min, forming (diphenylphosphino)methanol. The reaction mixture was transferred to a 250 mL three-necked flask containing a suspension of MMSN-NH<sub>2</sub> in dry and degassed toluene (150 mL) and stirred mechanically in an inert atmosphere under reflux for 24 h. The system was cooled to RT, separated magnetically, washed, and redispersed in toluene (100 mL).

### Supporting Pd(II) on MMSN-N-(PPh<sub>2</sub>)<sub>2</sub>

The phosphonated system MMSN-N-(PPh<sub>2</sub>)<sub>2</sub> in toluene was sonicated for 15 min and the Pd precursor (0.088 mmol) was added. The reaction mixture was stirred at RT for 24 h in an inert atmosphere. The catalytic system was separated magnetically, washed, and redispersed in toluene to reach 15 g suspension total. The Pd loading was determined by ICP-MS analysis.

### Synthesis of Si-Im

*N*-[3-(triethoxysilyl)propyl]-4,5-dihydroimidazole (14.5 mmol, 4 g) and  $\alpha, \alpha$ -dichloro-*m*-xylene (7.28 mmol, 1.27 g) in dry toluene (60 mL) were refluxed in an inert atmosphere for 48 h. The reaction mixture was cooled to RT, the solvent evaporated, and the resulting material dried in vacuo. A highly viscous yellow-orange product was obtained in 92% yield.

<sup>1</sup>H NMR (400 MHz,  $\text{CDCl}_3$ ):  $\delta = 0.61$  (t,  $J = 8.8$  Hz, 4H), 1.22 (t,  $J = 8$  Hz, 18H), 1.73–1.80 (m, 4H), 2.35 (m, 4H), 3.72 (t,  $J = 7.2$  Hz, 4H), 3.82 (q,  $J = 7.2$  Hz, 12H), 4.10 (t,  $J = 8.4$  Hz, 4H), 4.90 (s, 4H), 7.14–7.40 (m, 4H), 10.14 ppm (s, 2H); <sup>13</sup>C NMR (100 MHz,  $\text{CDCl}_3$ ):  $\delta = 7.3$ , 15.2, 18.3, 21.4, 48.0, 48.6, 50.7, 51.2, 58.4, 65.8, 125.2, 128.3, 128.9, 137.8, 159.0 ppm; elemental analysis calcd. (%) for  $\text{C}_{32}\text{H}_{60}\text{N}_4\text{O}_6\text{Si}_2$ : C, 53.09; H, 8.35; N, 7.74; Cl, 9.79; found: C, 49.79; H, 8.30; N, 7.19, Cl, 9.86.

### Synthesis of MMSN-Si-Im

A 250 mL three-necked flask was charged with MMSN in EtOH (150 mL) and Si-Im (0.42 mmol, 0.3 g). The mixture was stirred me-

chanically in an inert atmosphere and refluxed for 24 h. The system was cooled to RT and isolated magnetically, washed with EtOH and MeOH, and redispersed in dry MeOH (100 mL).

### Supporting Pd on MMSN-Si-Im

A suspension of MMSN-Si-Im in dry MeOH (10 mL) was sonicated for 60 min, followed by addition of KOtBu (0.7 mmol, 0.08 g). The suspension was stirred mechanically at RT in N<sub>2</sub> for 60 min, followed by addition of toluene (60 mL) and Pd precursor (0.067 mmol). The reaction mixture was stirred mechanically for a further 24 h at RT. The MMSN-Si-Im-Pd was isolated magnetically, washed with toluene, and redispersed in toluene to reach 15 g suspension total. The Pd loading was determined by ICP-MS analysis.

### Synthesis of MMSN-NiXantphos

To a suspension of MMSN dispersed in toluene (80 mL), (3-isocyanatopropyl)triethoxysilane (5 mmol, 0.9 g) was added and the mixture stirred mechanically in an inert atmosphere under reflux for 24 h. The isocyanato-modified MMSN was isolated magnetically, washed with toluene and redispersed in dry toluene (80 mL). 4,6-bis(diphenylphosphino)phenoxazine (0.3 g) was added to the suspension and the mixture refluxed for 24 h in an inert atmosphere. The system was cooled to RT and isolated magnetically, washed with toluene, and redispersed in dry toluene (100 mL).

Pd precursor (0.077 mmol) was supported on MMSN-NiXantphos in a similar manner as on MMSN-Si-NHC. The loading of the Pd was determined by ICP-MS analysis.

### General procedure for the catalyzed carbonylative Sonogashira reaction

A 25 mL glass-lined autoclave, equipped with a magnetic stirrer bar, was charged with aryl iodide, acetylene, base, and a dispersion of Pd supported on modified MMSN (1 g) in the desired solvent (4 mL).

The autoclave was sealed, flushed twice with CO, and pressurized to 40 or 400 psi. The reaction mixture was stirred at 25, 80, or 130 °C for 4, 12, or 24 h. The autoclave was cooled to RT and the CO gas released. The catalytic system was separated magnetically and the solution decanted and filtered through Celite. The solution was diluted with ether (10 mL), washed with H<sub>2</sub>O, dried over anhydrous MgSO<sub>4</sub>, and evaporated under reduced pressure.

### Reuse experiment

After completion of the carbonylative Sonogashira reaction of 4-iodoanisole with phenylacetylene catalyzed by MMSN-N-(PPh<sub>2</sub>)<sub>2</sub> to afford the desired product, the catalytic system was recovered by magnetic isolation and washed with DMA. The next reaction was performed with the same amounts of reagents and solvent under the same conditions as in the initial reaction.

### Acknowledgements

We acknowledge funding support from the Casali Foundation. S.N. is also grateful to the Ministry of Science, Culture and Sport of Israel for her fellowship.

**Keywords:** carbonylation • heterogeneous catalysis • nanoparticles • palladium • sol-gel processes

- [1] a) S. S. Stahl, *Angew. Chem. Int. Ed.* **2004**, *43*, 3400–3420; *Angew. Chem.* **2004**, *116*, 3480–3501; b) D. R. Jensen, J. S. Pugsley, M. S. Sigman, *J. Am. Chem. Soc.* **2001**, *123*, 7475–7476.
- [2] M. T. Oliveira, D. Audisio, S. Niyomchon, N. Maulide, *ChemCatChem* **2013**, *5*, 1239–1247.
- [3] Q.-A. Chen, Z.-S. Ye, Y. Duan, Y.-G. Zhou, *Chem. Soc. Rev.* **2013**, *42*, 497–511.
- [4] J. Pospech, I. Fleischer, R. Franke, S. Buchholz, M. Beller, *Angew. Chem. Int. Ed.* **2013**, *52*, 2852–2872; *Angew. Chem.* **2013**, *125*, 2922–2944.
- [5] A. Brennfürher, H. Neumann, M. Beller, *Angew. Chem. Int. Ed.* **2009**, *48*, 4114–4133; *Angew. Chem.* **2009**, *121*, 4176–4196.
- [6] a) C. C. C. Johansson Seechurn, M. O. Kitching, T. J. Colacot, V. Snieckus, *Angew. Chem. Int. Ed.* **2012**, *51*, 5062–5085; *Angew. Chem.* **2012**, *124*, 5150–5174; b) A. R. Kapdi, D. Prajapati, *RSC Adv.* **2014**, *4*, 41245–41259.
- [7] a) M. A. Barakat, M. H. H. Mahmoud, Y. S. Mahrous, *Appl. Catal. A* **2006**, *301*, 182–186; b) G. Kiss, *Chem. Rev.* **2001**, *101*, 3435–3456; c) G. Poli, G. Giambastiani, A. Heumann, *Tetrahedron* **2000**, *56*, 5959–5989.
- [8] a) C. J. Forsyth, J. Xu, S. T. Nguyen, I. A. Samdal, L. R. Briggs, T. Rundberget, M. Sandvik, C. O. Miles, *J. Am. Chem. Soc.* **2006**, *128*, 15114–15116; b) V. I. Dodero, L. C. Koll, M. Belén Faraoni, T. N. Mitchell, J. C. Podestá, *J. Org. Chem.* **2003**, *68*, 10087–10091; c) J. Marco-Contelles, E. de Opazo, *J. Org. Chem.* **2002**, *67*, 3705–3717.
- [9] G. T. Crisp, W. J. Scott, J. K. Stille, *J. Am. Chem. Soc.* **1984**, *106*, 7500–7506.
- [10] a) D. A. Alonso, C. Nájera, M. C. Pacheco, *J. Org. Chem.* **2004**, *69*, 1615–1619; b) M. W. Logue, K. Teng, *J. Org. Chem.* **1982**, *47*, 2549–2553; c) K. Y. Lee, M. J. Lee, J. N. Kim, *Tetrahedron* **2005**, *61*, 8705–8710.
- [11] T. Kobayashi, M. Tanaka, *J. Chem. Soc. Chem. Commun.* **1981**, 333–334.
- [12] M. S. Mohamed Ahmed, A. Mori, *Org. Lett.* **2003**, *5*, 3057–3060.
- [13] B. Liang, M. Huang, Z. You, Z. Xiong, K. Lu, R. Fathi, J. Chen, Z. Yang, *J. Org. Chem.* **2005**, *70*, 6097–6100.
- [14] T. Fukuyama, R. Yamaura, I. Ryu, *Can. J. Chem.* **2005**, *83*, 711–715.
- [15] a) G. J. Hutchings, *J. Mater. Chem.* **2009**, *19*, 1222–1235; b) G. V. Smith, F. Notheisz, *Heterogeneous Catalysis in Organic Chemistry*, Academic Press, San Diego, **1999**; c) M. Opanasenko, P. Stepnicka, J. Cejka, *RSC Adv.* **2014**, *4*, 65137–65162.
- [16] Y. Wang, J. Liu, C. Xia, *Tetrahedron Lett.* **2011**, *52*, 1587–1591.
- [17] W. Hao, J. Sha, S. Sheng, M. Cai, *J. Mol. Catal. A* **2009**, *298*, 94–98.
- [18] J. Liu, X. Peng, W. Sun, Y. Zhao, C. Xia, *Org. Lett.* **2008**, *10*, 3933–3936.
- [19] a) K. Philippot, P. Serp, *Concepts in Nanocatalysis*, Wiley-VCH, Weinheim, **2013**; b) P. Serp, K. Philippot, *Nanomaterials in Catalysis*, Wiley-VCH, Weinheim, **2013**; c) S. B. Kalidindi, B. R. Jagirdar, *ChemSusChem* **2012**, *5*, 65–75.
- [20] C. T. Kresge, M. E. Leonowicz, W. J. Roth, J. C. Vartuli, J. S. Beck, *Nature* **1992**, *359*, 710–712.
- [21] N. Z. Knežević, E. Ruiz-Hernandez, W. E. Hennink, M. Vallet-Regi, *RSC Adv.* **2013**, *3*, 9584–9593.
- [22] a) I. I. Slowing, J. L. Vivero-Escoto, C.-W. Wu, V. S. Y. Lin, *Adv. Drug Delivery Rev.* **2008**, *60*, 1278–1288; b) L. F. Giraldo, B. L. López, L. Pérez, S. Urrego, L. Sierra, M. Mesa, *Macromol. Symp.* **2007**, *258*, 129–141.
- [23] a) C. Yang, J. Wu, Y. Hou, *Chem. Commun.* **2011**, *47*, 5130–5141; b) W. Wu, Q. He, C. Jiang, *Nanoscale Res. Lett.* **2008**, *3*, 397–415.
- [24] a) S. Sun, H. Zeng, *J. Am. Chem. Soc.* **2002**, *124*, 8204–8205; b) S. F. Chin, S. C. Pang, C. H. Tan, *J. Mater. Environ. Sci.* **2011**, *2*, 299–302; c) Y.-h. Zheng, Y. Cheng, F. Bao, Y.-s. Wang, *Mater. Res. Bull.* **2006**, *41*, 525–529.
- [25] R. Massart, *IEEE Trans. Magn.* **1981**, *17*, 1247–1248.
- [26] a) T. E. Schmid, D. C. Jones, O. Songis, O. Diebolt, M. R. L. Furst, A. M. Z. Slawin, C. S. J. Cazin, *Dalton Trans.* **2013**, *42*, 7345–7353; b) C. Zhang, J. Liu, C. Xia, *Org. Biomol. Chem.* **2014**, *12*, 9702–9706; c) C. Romain, C. Fliedel, S. Bellemin-Lapponnaz, S. Dagorne, *Organometallics* **2014**, *33*, 5730–5739.
- [27] Z. Rohlík, P. Holzhauser, J. Kotek, J. Rudovsky, I. Nemeč, P. Hermann, I. Lukes, *J. Organomet. Chem.* **2006**, *691*, 2409–2423.

Received: March 31, 2015

Published online on June 26, 2015